Monthly Notices
of the
ROYAL ASTRONOMICAL SOCIETY
MNRAS **467,** 4431–4440 (2017) doi:10.1093/mnras/stx387

Asymptotic giant branch and super-asymptotic giant branch stars: modelling dust production at solar metallicity

F. Dell'Agli,[1,2]★ D. A. García-Hernández,[1,2] R. Schneider,[3] P. Ventura,[3] F. La Franca,[4] R. Valiante,[3] E. Marini[4] and M. Di Criscienzo[3]

[1]*Instituto de Astrofísica de Canarias, Vía Láctea s/n, E-38205 La Laguna, Tenerife, Spain*
[2]*Departamento de Astrofísica, Universidad de La Laguna (ULL), E-38206 La Laguna, Spain*
[3]*INAF – Osservatorio Astronomico di Roma, Via Frascati 33, 00040, Monte Porzio Catone (RM), Italy*
[4]*Dipartimento di Matematica e Fisica, Universita degli Studi 'Roma Tre', Via della Vasca Navale 84, I-00146 Roma, Italy*

Accepted 2017 February 10. Received 2017 February 8; in original form 2016 December 16

ABSTRACT

We present dust yields for asymptotic giant branch (AGB) and super-asymptotic giant branch (SAGB) stars of solar metallicity. Stars with initial mass $1.5\,M_\odot \leq M_{\rm ini} \leq 3\,M_\odot$ reach the carbon star stage during the AGB phase and produce mainly solid carbon and SiC. The size and the amount of the carbon particles formed follows a positive trend with the mass of the star; the carbon grains with the largest size ($a_{\rm C} \sim 0.2\,\mu$m) are produced by AGB stars with $M_{\rm ini} = 2.5$–$3\,M_\odot$, as these stars are those achieving the greatest enrichment of carbon in the surface regions. The size of SiC grains, being sensitive to the surface silicon abundance, remains at about $a_{\rm SiC} \sim 0.1\,\mu$m. The mass of carbonaceous dust formed is in the range 10^{-4}–$5 \times 10^{-3}\,M_\odot$, whereas the mass of SiC produced is 2×10^{-4}–$10^{-3}\,M_\odot$. Massive AGB/SAGB stars with $M_{\rm ini} > 3\,M_\odot$ experience hot bottom burning, which inhibits the formation of carbon stars. The most relevant dust species formed in these stars are silicate and alumina dust, with grain sizes in the range $0.1 < a_{\rm ol} < 0.15\,\mu$m and $a_{\rm Al_2O_3} \sim 0.07\,\mu$m, respectively. The mass of silicates produced spans the interval $3.4 \times 10^{-3}\,M_\odot \leq M_{\rm dust} \leq 1.1 \times 10^{-2}\,M_\odot$ and increases with the initial mass of the star.

Key words: stars: abundances – stars: AGB and post-AGB – stars: carbon – dust, extinction.

1 INTRODUCTION

In recent years there has been a growing interest in the evolution after the core helium-burning stage of low- and intermediate-mass stars ($M < 8\,M_\odot$). These late evolutionary phases, AGB or SAGB stars (for initial masses $6\,M_\odot < M < 8\,M_\odot$, which develop a O-Ne core), despite representing only a few per cent of the overall stellar lifetime, are of fundamental importance for understanding the feedback of these objects on the host environment. This is because AGB and SAGB stars are characterized by high mass-loss rates, which favour the loss of the whole external envelope, before the beginning of the planetary nebula and white dwarf evolution.

During the AGB phase, the stars eject gas with a chemical composition altered by internal nucleosynthesis processes, thus enriching the interstellar medium. Several theoretical studies have presented mass- and metallicity-dependent AGB stellar yields (see, among others, Cristallo et al. 2009, 2015; Doherty et al. 2014; Karakas 2010, 2014; Karakas & Lattanzio 2014; Karakas & Lugaro 2016; Ventura et al. 2013, 2014; Di Criscienzo et al. 2016). These works derived several similarities but also significant differences in the predicted yields. These differences are mostly a result of the different descriptions of convection used, in terms both of the efficiency of convective transport and of the treatment of the convective/radiative interface.

A strong interest in AGB stars is also motivated by the thermodynamical structure of the circumstellar envelope, which has proved to be an environment extremely favourable to the condensation of gaseous molecules into dust particles. The surface layers of these stars are sufficiently cool ($T_{\rm eff} < 4000$ K) to allow dust formation at typical distances of 3–10 stellar radii from the surface, where the densities are high enough ($\rho > 10^{-14}\,{\rm g\,cm^{-3}}$, Gail & Sedlmayr 1985) to allow the formation of meaningful quantities of dust.

The pioneering investigations by the Heidelberg group (Ferrarotti & Gail 2001, 2002, 2006) set up a framework for modelling dust formation in the circumstellar envelope of AGB stars: the schematisation adopted is based on the assumption that the wind expands isotropically from the stellar surface, under the push of radiation pressure, acting on the newly formed dust grains. While interesting improvements to this basic treatment, accounting for the effects of shocks coupled to the AGB evolution are in progress

★ E-mail: fdellagli@iac.es

© 2017 The Authors
Published by Oxford University Press on behalf of the Royal Astronomical Society

Downloaded from https://academic.oup.com/mnras/article/467/4/4431/3072233 by INAF Roma (Osservatorio Astronomico di Roma) user on 08 October 2020

(Marigo et al. 2016), this approach is at present the only way to allow the description of dust formation in the winds of stars of different mass and chemical composition, extended over the whole AGB phase. Indeed, different research groups have modelled the formation and growth of solid particles in the wind of low-metallicity AGB stars, calculating the dust yields from this class of objects (Ventura et al. 2012a,b, 2014; Di Criscienzo et al. 2013; Nanni et al. 2013, 2014). These models have been successfully used to interpret the near- and mid-infrared observations (mainly obtained with the *Spitzer Space Telescope*) of evolved stars in the Magellanic Clouds (Dell'Agli et al. 2014b, 2015a,b; Nanni et al. 2016) and in the Local Group (LG) galaxy IC 1613 (Dell'Agli et al. 2016). An important outcome of these investigations was the characterization of the individual sources observed, in terms of the mass, formation epoch and chemical composition of their progenitors. Furthermore, these studies allowed important information to be inferred on the past history of the host galaxy (particularly the star formation history and the mass–metallicity relationship) and provided valuable constraints on the physical mechanisms relevant to understanding the main evolutionary properties of AGB stars.

As mentioned above, these works have so far been based on low-metallicity extragalactic AGB stars. This is partly owing to the fact that the distances to Galactic sources are basically unknown or very uncertain, so that interpretation of the observations is quite difficult. This limitation will be largely overcome by the results of the *Gaia* mission, because the parallaxes – and so the distances and luminosities – will be measured with high accuracy for an important fraction of Galactic AGB stars, including those exhibiting a large degree of obscuration. This will open new frontiers in the AGB field, because the sample of Galactic AGB stars is much larger and extends to a wider metallicity range than the AGB population of the Magellanic Clouds and other LG galaxies.

In order to be ready for the *Gaia* challenge, we have recently extended the AGB models, until now limited to metallicities $Z \leq 8 \times 10^{-3}$, to solar metallicity (Di Criscienzo et al. 2016, hereinafter DC16). In DC16 we presented the main evolutionary properties of the solar-metallicity AGB models as well as the chemistry of the gas ejected in the interstellar medium. Here we focus on the dust formation properties and present new dust yields based on a self-consistent coupling of the wind description with the DC16 AGB evolutionary models. In addition, these solar-metallicity AGB dust models will be essential for interpreting the rich data set of IR photometric observations (e.g. from space missions such as *MSX*, *AKARI* and *WISE*) of Galactic sources as well as the already available *Spitzer* photometric observations of evolved stars in nearby high-metallicity galaxies such as M31 (Mould et al. 2008), M33 (McQuinn et al. 2007; Javadi, van Loon & Mirtorabi 2011a,b; Javadi et al. 2015) and M32 (e.g. Jones et al. 2015). The results presented here and in our previous papers of this series (Ventura et al. 2012a,b; Di Criscienzo et al. 2013; Ventura et al. 2014), complemented by a new mass- and metallicity-dependent supernova (SN) dust grid (Marassi et al. 2014, 2015; Bocchio et al. 2016, Marassi et al. in prep), will allow us to assess fully the role of AGB stars as cosmic dust polluters, in present-day galaxies (Schneider et al. 2014) as well as at very high redshifts (Valiante et al. 2009, 2011; Mancini et al. 2015, 2016).

2 DUST FORMATION MODEL

We describe the growth of dust particles in the circumstellar envelope of AGB stars by means of the schematisation introduced by the Heidelberg group (Ferrarotti & Gail 2001, 2002, 2006). We provide here a short description of the basic concepts upon which the modelling of the wind dynamics and of the dust formation process is based; we direct the interested reader to the previous works on this topic (Ventura et al. 2012a,b; Di Criscienzo et al. 2013; Ventura et al. 2014; Dell'Agli et al. 2014a), which include the full set of equations used and a more exhaustive discussion on this approach.

The wind is assumed to expand isotropically from the surface of the star. Dust formation occurs once the growth rate of solid grains exceeds the rate of destruction (hereafter the decomposition rate). The growth rate is determined by the deposition efficiency of gaseous molecules on the already formed solid particles. For each dust species, the decomposition rate is found via evaluation of the vapour pressures of the individual molecular species involved, under conditions of thermodynamic equilibrium (Gail & Sedlmayr 1999).

The description of the wind is self-consistently coupled to the results of stellar evolution: the input parameters entering dust formation, namely the mass (M), luminosity (L), effective temperature ($T_{\rm eff}$), radius (R_*), mass-loss rate ($\dot{M}$) and surface chemical composition of the star, are the natural outputs of AGB evolutionary modelling.

The kind of particles formed in the circumstellar envelope depends on the surface chemical composition of the star, mainly on the surface carbon-to-oxygen (C/O) ratio. This is because the CO molecule is extremely stable (Sharp & Huebner 1990), and thus the least abundant element between carbon and oxygen is locked into CO molecules. Based on stability arguments, we assume that in carbon-rich environments the species of dust formed are solid carbon, solid iron and silicon carbide, whereas in M stars the formation of silicates (olivine, pyroxene and quartz), solid iron and alumina dust is considered (Sharp & Huebner 1990; Ferrarotti & Gail 2006). For each dust species it is possible to identify the key element, which is the element that is least abundant among the various chemical species required to form the solid particles: such a key element is extremely important, as it determines the largest amount of a specific kind of dust particle that can be formed. A list of the dust species considered here, with the reactions of formation, the key elements and the sticking coefficients adopted, is shown in table 1 of Ventura et al. (2014).[1]

3 SOLAR METALLICITY AGB STARS

The AGB evolutionary models calculated with the code ATON (Canuto & Mazzitelli 1991) and used in the present work have been recently published by DC16. The models span the range of initial masses $1\,{\rm M}_\odot \leq M_{\rm ini} \leq 8\,{\rm M}_\odot$. The upper limit is determined by the core collapse via electron capture experienced by $M_{\rm ini} > 8\,{\rm M}_\odot$ stars. During the AGB phase, the stars evolve on a degenerate core composed of carbon and oxygen, with the exception of stars with mass greater than $\sim$6.5 ${\rm M}_\odot$, which form a core composed of oxygen and neon (the so-called SAGB stars), owing to an off-centre ignition of carbon in conditions of partial degeneracy (García-Berro & Iben 1994; García-Berro, Ritossa & Iben 1997; Siess 2006, 2007, 2009, 2010). The interested reader is referred to DC16 for an exhaustive discussion on the evolutionary properties of these stars. Here we provide only a brief summary of the physical and chemical evolutionary aspects most relevant to the dust formation process in their winds.

[1] Following the analysis published in Dell'Agli et al. (2014a), where different values of the sticking coefficient for the alumina dust were explored, we adopted the value 0.1, which is consistent with the recent laboratory measurements by Takigawa et al. (2015).

Downloaded from https://academic.oup.com/mnras/article/467/4/4431/3072233 by INAF Roma (Osservatorio Astronomico di Roma) user on 08 October 2020

Stars of initial mass $M_{\rm ini} \geq 3.5\,{\rm M}_{\odot}$, which we term 'massive AGB/SAGB stars', experience hot bottom burning (hereinafter HBB) at the base of the outer convective envelope (Renzini & Voli 1981). The activation of proton-capture nucleosynthesis at the bottom of the external mantle leads to a considerable increase in the luminosity of the star (Blöcker & Schöenberner 1991), resulting in significant deviations from the classic core mass–luminosity relationship (Paczynski 1970). The largest luminosities reached range from $L \sim 2 \times 10^4\,L_{\odot}$, for $M_{\rm ini} = 3.5\,{\rm M}_{\odot}$, to $L \sim 10^5\,L_{\odot}$, for $M_{\rm ini} = 8\,{\rm M}_{\odot}$. The temperatures at which the bottom of the surface convective zone is exposed, which affect the degree of nucleosynthesis experienced, span the range [30–100] MK (see fig. 1 in DC16).

Regarding the chemistry, massive AGB/SAGB stars never reach the C-star stage, because the surface carbon is destroyed at the base of the convective envelope by proton-capture reactions, which prevent the achievement of the C/O > 1 condition. Owing to the ignition of CN cycling, the ejecta from these stars are nitrogen-rich (with an overall nitrogen increase slightly below a factor of 10 with respect to the initial abundance) and carbon-poor, with the carbon content being one order of magnitude smaller than that of the original gas out of which the stars formed. Unlike lower-metallicity AGB stars, in this case the HBB temperatures are below 100 MK, which is reflected in a modest (below ∼20 per cent) depletion of oxygen and magnesium and a negligible production of aluminium. Sodium is produced in significant quantities, with an average sodium increase in the ejecta of a factor of ∼4 (see figs 8 and 9 in DC16).

The evolution of AGB models with $M_{\rm ini} < 3.5\,{\rm M}_{\odot}$, which we term 'low-mass AGB stars', is very different from that of their higher-mass counterparts. This is because the core mass is $<0.8\,{\rm M}_{\odot}$, which is too small to activate HBB (Ventura et al. 2013). In this case, the only physical mechanism able to alter the surface chemical composition is the third dredge-up (TDU), which results in a gradual increase in the surface carbon and, eventually, in the formation of a C- star (C/O > 1).

Regarding the physics, the achievement of the C-star stage causes a considerable increase in the surface molecular opacities, which favours a general cooling and a considerable expansion of the external regions (Marigo 2002; Ventura & Marigo 2009, 2010). The stellar effective temperature ($T_{\rm eff}$) decreases down to ∼1900 K, in conjunction with the maximum surface carbon abundance. Consequently, the outermost regions of the star become less and less gravitationally bound and the mass-loss rate increases. After the C-star stage is reached, the evolutionary times become short, and the relative duration of the C-star phase is below 15 per cent with respect to the entire AGB phase (see table 1 in DC16).

The surface chemical composition of low-mass AGB stars is entirely dominated by the effects of TDU. The gas lost by these stars is enriched in carbon, with a maximum increase by a factor of ∼3 achieved in the $M_{\rm ini} = 3\,{\rm M}_{\odot}$ model. The final surface carbon abundances range from $X_{\rm C} = 7.3 \times 10^{-3}$ for $M_{\rm ini} = 1.5\,M_{\odot}$ to $X_{\rm C} = 9.7 \times 10^{-3}$ for $M_{\rm ini} = 3\,M_{\odot}$. The enrichment in carbon increases with $M_{\rm ini}$ because more massive stars are exposed to a higher number of TDU events before the envelope is completely lost.

4 DUST PRODUCTION

As discussed in Section 2, the kind of dust grains (i.e. their specific chemical composition) formed in the wind of AGB stars is determined mainly by the surface C/O ratio: oxygen-rich stars produce silicate and alumina (Al_2O_3) dust grains; C-stars produce solid carbon and silicon carbide (SiC) grains.

The surface chemical composition of solar-metallicity AGB stars is extremely sensitive to the initial mass (see Section 3): stars with $1.5\,{\rm M}_{\odot} \leq M_{\rm ini} \leq 3\,{\rm M}_{\odot}$ become carbon stars,[2] while their higher-mass counterparts evolve as M stars for the whole AGB phase. This dichotomy is reflected in the dust composition, which is dominated by silicates in massive AGB/SAGB stars and by solid carbon in the low-mass domain. In the following, we analyse these two groups separately. We do not discuss stars with $M_{\rm ini} < 1.5\,{\rm M}_{\odot}$, because they produce only a negligible amount of silicates during their life.

4.1 Dust production in massive AGB/SAGB stars

Fig. 1 shows the variation of the luminosity, the size of the dust particles formed in the wind, the fraction of the key species (silicon and aluminium) condensed into dust, and the dust mass-loss rate (split into the silicate and the alumina dust contributions), for massive AGB/SAGB stars.

For these objects, the production of dust is modulated by the luminosity (Ventura et al. 2012a,b). The larger L is, the larger the mass-loss rate, and the higher the density of the gas (see equation 2 in Ventura et al. 2014). This favours dust production, owing to the larger number of gaseous molecules available to form dust.

As shown in the top-left panel of Fig. 1, the luminosity increases during the initial AGB phases owing to the increase in the core mass. This trend is reversed at a given stage during the AGB evolution because of the progressive consumption of the external mantle, which favours the general cooling of the whole external structure. This behaviour is reflected in the amount and the size of the dust grains produced during the AGB lifetime. The silicate grains with the largest size are formed during the highest-luminosity phases (see the top-right panel in Fig. 1).[3] This is the phase where we expect massive AGB/SAGB stars to show the strongest IR emission, as this is sensitive to the amount of dust in the circumstellar envelope.

Because higher-mass stars evolve at greater luminosities, olivine grains with the largest size, $a_{\rm ol} \sim 0.15\,\mu$m, are produced by AGB stars with initial mass close to the threshold to undergo core collapse, namely $M_{\rm ini} \sim 8\,{\rm M}_{\odot}$. Generally speaking, most of the olivine grains formed in the wind of massive AGB/SAGB stars have dimensions in the range $0.1\,\mu{\rm m} < a_{\rm ol} < 0.15\,\mu$m, while pyroxene and quartz grains can be as small as ∼0.07 μm and $< 0.05\,\mu$m, respectively.

The fraction of silicon condensing into solid particles (see the bottom-left panel in Fig. 1) is [20–40] per cent. In the case of stars with initial mass $M_{\rm ini} > 4\,{\rm M}_{\odot}$ these percentages are significantly smaller than those in the alumina dust case, during almost the entire AGB phase. This is because of the large extinction coefficient of silicates, which favours a significant acceleration of the wind as soon as silicate particles begin to form. Under these conditions, mass continuity leads to a sudden drop in the density of the gas, which prevents the further formation of dust.

Massive AGB/SAGB stars, particularly during the highest-luminosity phases, eject great quantities of silicates into the interstellar medium (see the bottom-right panel of Fig. 1). The rate

[2] As discussed in DC16, stars of mass below $1.5\,{\rm M}_{\odot}$ never reach the C-star stage, because they loose the whole external mantle before the amount of surface carbon exceeds that of oxygen.

[3] For the sake of clarity, we show only the dominant silicate species, i.e. olivine. We discuss the properties of the other dust species in the text.

Downloaded from https://academic.oup.com/mnras/article/467/4/4431/3072233 by INAF Roma (Osservatorio Astronomico di Roma) user on 08 October 2020

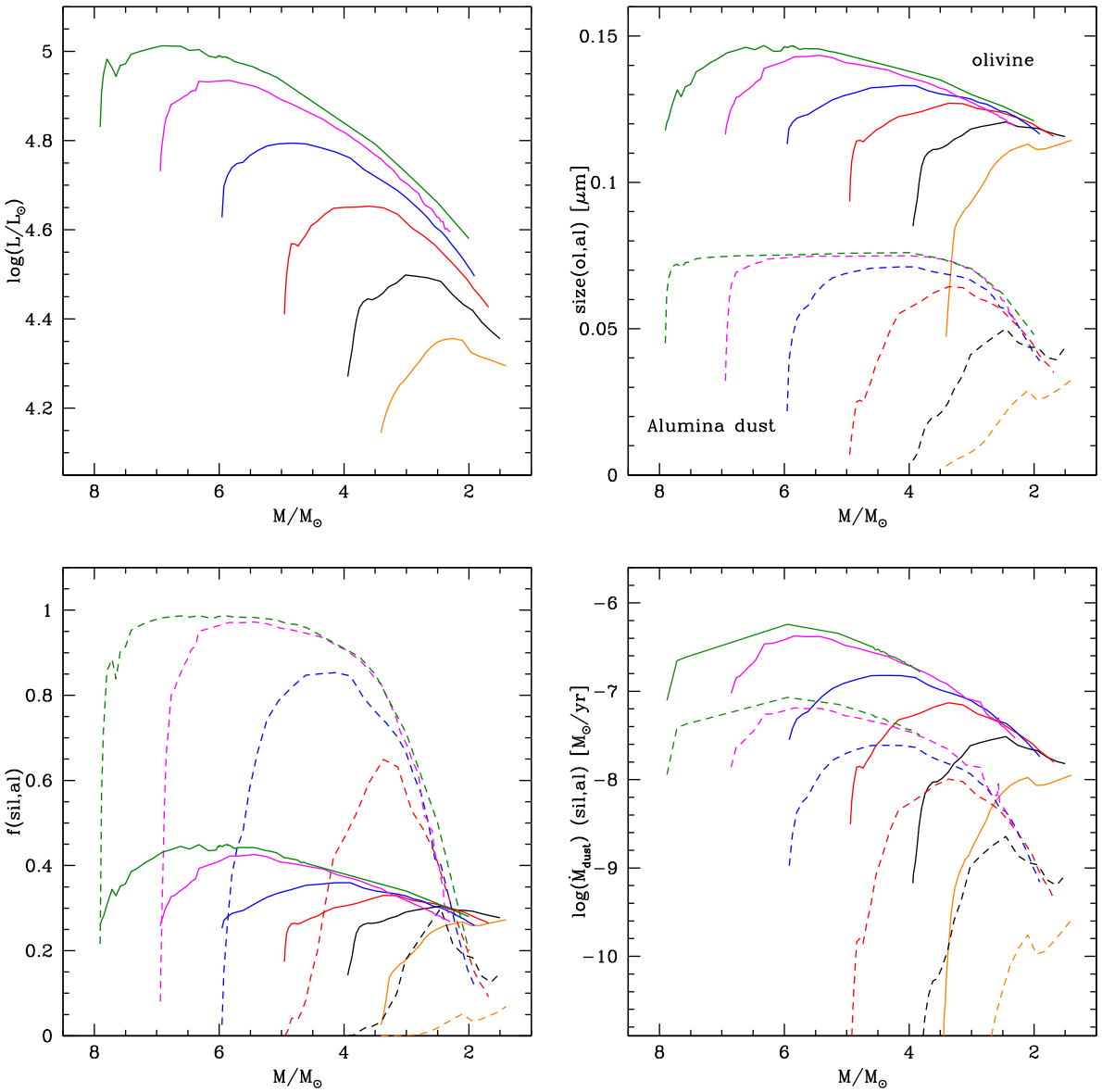

Figure 1. The variation during the AGB phase of the physical and dust properties of massive AGB/SAGB stars, with initial mass in the range [3.5–8] $M_\odot$, shown by the coloured lines from orange to green, respectively. The current mass of the star (decreasing during the evolution) is displayed on the abscissa. The quantities shown in the four panels are: luminosity (top-left); the size of olivine and Al_2O_3 grains (top-right, solid and dashed lines, respectively); the fraction of silicon condensed into silicates and the fraction of aluminium condensed into alumina dust (bottom-left, solid and dashed lines, respectively); the silicate and alumina dust mass-loss rates (bottom-right, solid and dashed lines, respectively). A coloured version of this plot is available online.

at which silicate dust is ejected is in the range $10^{-8}\,M_\odot\,yr^{-1} < \dot{M}_{sil} < 10^{-6}\,M_\odot\,yr^{-1}$.

The behaviour of alumina dust is different from that of silicates. Al_2O_3 is more thermodynamically stable (Sharp & Huebner 1990), and thus it forms closer to the stellar surface (Dell'Agli et al. 2014a). This compound is rather transparent to the electromagnetic radiation, so no significant acceleration of the gas occurs when alumina dust is formed. Therefore, it is possible that high fractions of the aluminium available condense into dust. This is shown in the bottom-left panel of Fig. 1, where it can be seen that during the highest luminosity phases of SAGB stars ($6\,M_\odot \le M_{ini} \le 8\,M_\odot$) more than ∼80 per cent of aluminium is condensing into dust. The largest sizes of alumina dust particles, $a_{Al_2O_3} \sim 0.07$ μm (see top-right panel in Fig. 1), are reached during the phases when all the aluminium available is locked into Al_2O_3 grains. The alumina dust contribution to the total dust production rate is approximately one order of magnitude smaller than that of the silicates, with Al_2O_3 mass-loss rates of $\dot{M}_{Al_2O_3} < 10^{-7}\,M_\odot\,yr^{-1}$ in all cases (see the bottom-right panel in Fig. 1).

When comparing the formation process of silicate and alumina dust, it is important to note that the main limiting factor to the growth of silicates is the large wind acceleration caused by radiation pressure, which leads to a sudden drop of the gas density. Conversely, the main limiting factor to the growth of alumina grains is the amount of aluminium present in the surface regions of the star.

Alumina dust starts to condense at distances below ∼3 $R_\star$ from the stellar surface, whereas silicate particles form in a region between 4 and 9 $R_\star$. The location of the condensation zone of silicates is sensitive to the initial mass of the star, being closer to the stellar surface the lower M_{ini} is. In [6–8] $M_\odot$ SAGB stars, the

Downloaded from https://academic.oup.com/mnras/article/467/4/4431/3072233 by INAF Roma (Osservatorio Astronomico di Roma) user on 08 October 2020

Table 1. Dust mass produced by low-mass AGB and massive AGB/SAGB models of solar metallicity. The initial stellar mass $M_{\rm ini}$ is shown in the first column. The total mass of dust, $M_{\rm d}$, and the mass of the several dust species: olivine ($M_{\rm ol}$), pyroxene ($M_{\rm py}$), quartz ($M_{\rm qu}$), alumina dust($M_{\rm Al_2O_3}$), solid iron ($M_{\rm ir}$), solid carbon ($M_{\rm C}$) and silicon carbide ($M_{\rm SiC}$) are also shown. All masses are expressed in solar units.

$M_{\rm ini}$	$M_{\rm d}$	$M_{\rm ol}$	$M_{\rm py}$	$M_{\rm qu}$	$M_{\rm Al_2O_3}$	$M_{\rm ir}$	$M_{\rm C}$	$M_{\rm SiC}$
1.5	5.11×10^{-4}	8.45×10^{-5}	2.95×10^{-5}	9.40×10^{-6}	4.42×10^{-8}	1.16×10^{-4}	5.61×10^{-5}	2.08×10^{-4}
1.75	7.17×10^{-4}	2.81×10^{-5}	1.18×10^{-5}	7.67×10^{-6}	1.72×10^{-8}	2.74×10^{-4}	2.82×10^{-4}	1.05×10^{-4}
2.0	2.34×10^{-3}	6.36×10^{-6}	2.36×10^{-6}	8.71×10^{-7}	2.18×10^{-9}	1.28×10^{-3}	9.41×10^{-4}	1.10×10^{-4}
2.25	3.23×10^{-3}	1.81×10^{-6}	7.05×10^{-7}	4.31×10^{-7}	1.31×10^{-9}	9.69×10^{-5}	2.53×10^{-3}	6.01×10^{-4}
2.5	4.19×10^{-3}	1.62×10^{-7}	6.06×10^{-8}	2.35×10^{-8}	2.29×10^{-10}	2.29×10^{-5}	3.27×10^{-3}	8.93×10^{-4}
3.0	6.05×10^{-3}	5.24×10^{-7}	2.08×10^{-7}	8.84×10^{-8}	5.04×10^{-10}	2.07×10^{-5}	5.09×10^{-3}	9.40×10^{-4}
3.5	2.37×10^{-3}	1.53×10^{-3}	4.44×10^{-4}	5.35×10^{-5}	2.96×10^{-5}	2.96×10^{-4}	–	–
4.0	3.20×10^{-3}	2.33×10^{-3}	6.00×10^{-4}	3.96×10^{-5}	1.15×10^{-4}	1.09×10^{-4}	–	–
4.5	3.74×10^{-3}	2.75×10^{-3}	6.74×10^{-4}	3.63×10^{-5}	1.95×10^{-4}	8.11×10^{-5}	–	–
5.0	4.48×10^{-3}	3.31×10^{-3}	7.70×10^{-4}	3.28×10^{-5}	3.07×10^{-4}	6.19×10^{-5}	–	–
5.5	5.34×10^{-3}	3.91×10^{-3}	8.70×10^{-4}	2.95×10^{-5}	4.75×10^{-4}	5.08×10^{-5}	–	–
6.0	6.16×10^{-3}	4.47×10^{-3}	9.61×10^{-4}	2.92×10^{-5}	6.43×10^{-4}	5.08×10^{-5}	–	–
6.5	7.72×10^{-3}	5.60×10^{-3}	1.12×10^{-3}	2.61×10^{-5}	9.15×10^{-4}	5.74×10^{-5}	–	–
7.0	8.20×10^{-3}	5.92×10^{-3}	1.16×10^{-3}	2.62×10^{-5}	1.04×10^{-3}	5.82×10^{-5}	–	–
7.5	1.05×10^{-2}	7.51×10^{-3}	1.36×10^{-3}	2.20×10^{-5}	1.51×10^{-3}	7.98×10^{-5}	–	–
8.0	1.14×10^{-2}	8.22×10^{-3}	1.43×10^{-3}	2.07×10^{-5}	1.65×10^{-3}	8.41×10^{-5}	–	–

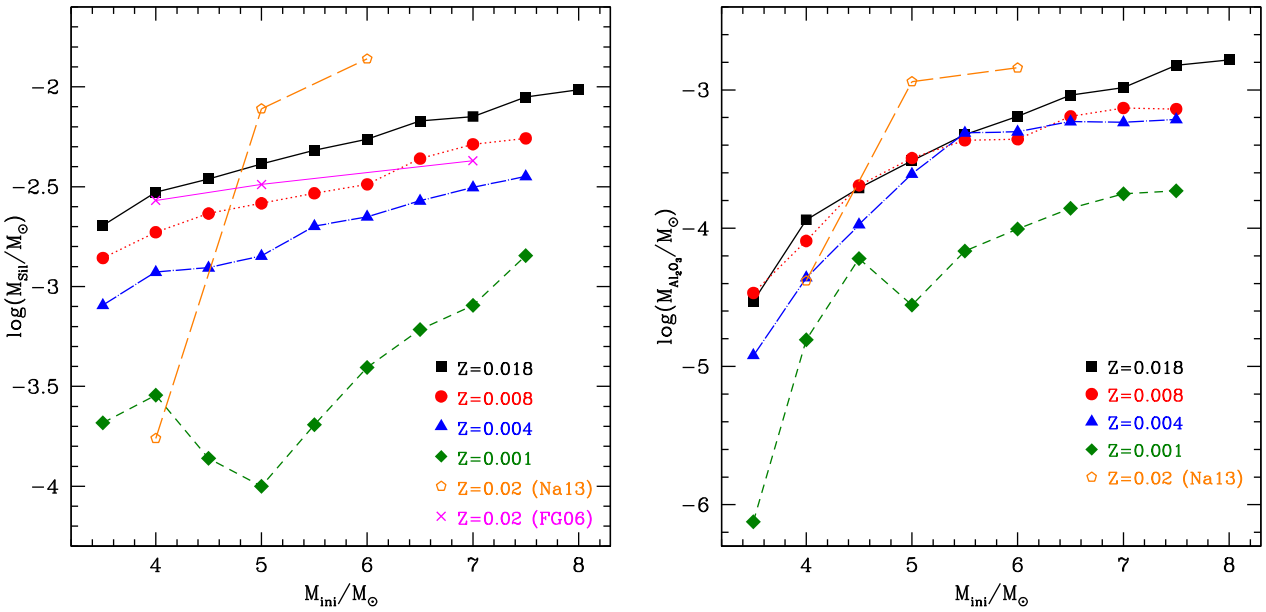

Figure 2. The masses of silicate (left panel) and alumina (right panel) dust produced by solar-chemistry AGB stars of different masses are indicated with full squares and connected with a solid line. Results for lower-metallicity models with $Z = 10^{-3}$, 4×10^{-3}, 8×10^{-3} are indicated, respectively, with full green diamonds (dashed line), full blue triangles (dot–dashed line) and full red points (dotted line). The results from Nanni et al. (2013, Na13) and from Ferrarotti & Gail (2006, FG06) for $Z = 0.02$ are shown, respectively, with open orange points, connected with a long-dashed line, and with magenta crosses, connected with a solid line (note that the formation of Al_2O_3 particles is not described in Ferrarotti & Gail 2006).

formation of alumina dust in an internal zone of the circumstellar envelope, despite not being sufficient to accelerate the wind, produces a steep gradient of the optical depth (see equation 4 in Ventura et al. 2014). This increases the gas temperature (equation 3 in Ventura et al. 2014), moving the silicate dust condensation zone to more external regions (between 6 and 9 $R_\star$ from the stellar surface). This effect is negligible in massive AGB stars with $M_{\rm ini} \lesssim 5\,{\rm M}_\odot$, and the silicate dust formation takes place in a more internal region (between 4 and 6 $R_\star$).

The masses of silicate and alumina dust produced by solar-metallicity AGB stars are listed in Table 1. In Fig. 2 they are compared with results from lower-Z AGB models (Ventura et al. 2012a,b; Di Criscienzo et al. 2013; Ventura et al. 2014). We find that the amount of silicate and alumina dust increases with the initial mass of the star. The mass of produced silicate dust ranges from $M_{\rm sil} \sim 2 \times 10^{-3}\,{\rm M}_\odot$ ($M_{\rm ini} = 3.5\,{\rm M}_\odot$) to $M_{\rm sil} \sim 9.7 \times 10^{-3}\,{\rm M}_\odot$ ($M_{\rm ini} = 8\,{\rm M}_\odot$). The amount of formed alumina dust spans the mass interval $3 \times 10^{-5} < M_{\rm Al_2O_3} < 1.7 \times 10^{-3}\,{\rm M}_\odot$. Considering both dust contributions (alumina and silicates), we find for the present models a dust-to-gas ratio (δ) of $\log(\delta) \sim -3$. As discussed earlier in this section, the mass-loss rate is the key parameter determining the overall dust production in massive AGB/SAGB stars. This is the reason why δ turns out to be only mildly dependent on $M_{\rm ini}$.

The left panel of Fig. 2 shows that the mass of silicates scales almost linearly with Z. This is caused by the larger amount of silicon available in higher-metallicity stars. The trend of the alumina dust

Downloaded from https://academic.oup.com/mnras/article/467/4/4431/3072233 by INAF Roma (Osservatorio Astronomico di Roma) user on 08 October 2020

mass with metallicity is still positive but less straightforward, the results being less sensitive to Z. The higher efficiency of HBB in lower-metallicity models favours alumina dust production (i.e. more gaseous Al is available to form Al-based dust grains) and partially compensates the effect of the lower metallicity. On the other hand, the exhaustion of the gaseous aluminium available for condensation into dust sets an upper limit to the amount of Al_2O_3 formed.

The present results indicate that massive AGB stars experiencing HBB are the main manufacturers of alumina dust and silicates. This is in good agreement with the recent findings by Lugaro et al. (2017): by comparing the $^{17}O/^{16}O$ isotopic ratio in presolar grains with the new $^{17}O(p,\alpha)^{14}N$ proton-capture rate (Bruno et al. 2016), these authors found that massive AGB stars experiencing HBB are the stars most likely to be responsible for the formation of Al-rich oxides and silicate grains.

4.2 Dust production in low-mass AGB stars

Low-mass AGB stars produce negligible quantities of silicate and alumina dust grains during the initial part of their AGB evolution, before becoming C-stars. This is because of the low mass-loss rate and luminosity experienced. The dust formed in the circumstellar envelope of these stars is produced mainly during the C-rich phase and is composed of solid carbon and SiC.

While luminosity is the main factor affecting dust formation in massive AGB/SAGB stars, the formation of dust in low-mass stars is guided by the amount of carbon available in the envelope. Therefore, the quantity of dust formed increases during the C-star phase, as more and more carbon is transported to the stellar surface, owing to the effects of repeated TDU episodes. The increase in the surface carbon is accompanied by an increased cooling of the external regions, which leads to a significant decrease in the effective temperature and to an increase in the mass-loss rate (Marigo 2002; Ventura & Marigo 2009, 2010). This additional factor, for the reasons outlined in the previous sections, further favours the formation and growth of C-based dust particles.

Fig. 3 shows the variation of the surface C/O ratio, the size of carbon and SiC dust grains formed, the fraction of carbon and silicon condensed into dust, and the mass-loss rate of carbon and SiC dust, during the AGB phase of stars with initial mass $1.5\,M_\odot \leq M_{\rm ini} \leq 3\,M_\odot$.

The size of the carbon dust grains increases during the AGB phase (see top-right panel) as a consequence of the increase in the surface carbon abundance (top-left panel). Therefore, carbon grains with the largest size form during the final AGB phases, when the surface carbon mass fraction reaches the maximum value. The typical size of carbon grains is in the range $0.05\,\mu m < a_C < 0.25\,\mu m$, and it increases with the initial stellar mass, because stars of higher mass experience a higher number of TDU episodes, accumulating a higher abundance of carbon in the external layers (DC16). This is clear from Fig. 3 (top-right panel), where models with $M_{\rm ini} < 2\ M_\odot$, whose surface C/O barely exceeds unity, form smaller dust grains than their more massive counterparts.

The fraction of gaseous carbon condensed into dust, shown in the botton-left panel of Fig. 3, ranges from ∼10 to ∼35 per cent. The upper limit is motivated by the large values of the carbon dust extinction coefficients, which favour a rapid acceleration of the wind once carbon grains begin to form. This is similar to the effect on the dynamics of the wind triggered by the formation of silicates in the circumstellar envelope of massive AGB/SAGB stars.

A different behaviour is found for SiC. Although SiC is more stable and it is formed in more internal circumstellar regions (with higher density), the growth of SiC particles never exceeds the threshold value of $a_{\rm SiC} \sim 0.1\,\mu m$ (see the top-right panel in Fig. 3), which corresponds to the situation where ∼55 per cent of gaseous silicon is condensed into dust (see the bottom-left panel in Fig. 3). This is the largest amount of silicon available to form dust, because of the high stability of the SiS molecule, which means that ∼45 per cent of the total silicon in the envelope is locked into gaseous SiS (Ferrarotti & Gail 2006).

The region where SiC forms is $\sim[3.5–5.5]R_\star$ from the surface of the star, to be compared with the larger distances, $\sim[5.5–9]R_\star$, of the carbon condensation zone.

Similarly to what is found for oxygen-rich stars, the formation of the most stable dust species, namely SiC, favours an increase in the optical depth, so that solid carbon condensation takes place in a more external region of the wind. This effect becomes more and more important as the stars evolve through the AGB, because the density of the wind increases towards the final evolutionary phases. In stars with initial mass $M_{\rm ini} < 2\,M_\odot$, which achieve only a modest C/O ratio during the AGB evolution, the residual gaseous carbon in the wind after SiC formation in the internal regions of the circumstellar envelope is such that the size of the carbon grains formed is barely equal to or is even smaller than that of SiC grains.

The rates at which carbon and SiC dust are ejected into the interstellar medium increase during the AGB evolution. The largest values, attained in the final evolutionary phases, are of the order of $\dot{M}_C \sim 10^{-6}\dot{M}_\odot\ {\rm yr}^{-1}$ for carbon dust and of $10^{-8}\dot{M}_\odot\ {\rm yr}^{-1} < \dot{M}_{\rm SiC} < 10^{-7}\dot{M}_\odot\ {\rm yr}^{-1}$ for SiC (see the bottom-right panel in Fig. 3).

The masses of carbon and SiC dust produced by solar-metallicity low-mass AGB stars are shown in Fig. 4 and compared with the corresponding dust masses from lower-metallicity stars. The mass of carbon dust is in the range $10^{-4}\,M_\odot < M_C < 10^{-2}\,M_\odot$. The trend with $M_{\rm ini}$ is positive, as expected (see the discussion above). The trend with metallicity, however, is not trivial. For stars with $M_{\rm ini} \leq 2\,M_\odot$, the amount of carbon dust produced by solar-metallicity models is smaller than what is found at lower Z. Because of the higher initial amount of oxygen, the C-star stage is attained in a more advanced AGB phase, and the carbon excess with respect to oxygen is generally smaller. For stars with $M_{\rm ini} \sim [2.5-3]\,M_\odot$, this is compensated by the higher temperatures at the base of the envelope attained by lower-metallicity stars of the same mass, which favours the ignition of a soft HBB, preventing the accumulation of high quantities of carbon in the surface regions.

The dust-to-gas ratio of C-stars ranges from $\log(\delta) \sim -3$, at the beginning of the carbon-rich phase, up to $\log(\delta) \sim -2.4$, achieved during the final phases of AGB stars with $M_{\rm ini} = [2.5-3]\,M_\odot$.

The mass of SiC produced is in the range $10^{-4}\,M_\odot < M_{\rm SiC} < 10^{-3}\,M_\odot$. Although the abundance of the key species (silicon in this case) results to be proportional to the metallicity, this is not the case for $M_{\rm SiC}$. For $M_{\rm ini} \leq 2\,M_\odot$, $M_{\rm SiC}$ is comparable to what is found for the $Z = (4-8)\times10^{-3}$ models, whereas for higher masses the SiC dust mass for $Z = 0.018$ is slightly larger than that for lower-Z AGB stars. The reasons for this behaviour are the same as those illustrated above to explain the trend of carbon dust with metallicity. In addition, a significant fraction of the mass of the envelope is lost when the stars are still oxygen-rich, and thus the mass lost by the star during the phase when SiC dust is formed is smaller. This effect partly counterbalances the higher silicon abundance in the star.

Regarding what affects the relative contributions of solid carbon and SiC to the overall dust production by low-mass AGB stars, we find that the individual contributions of the two species are sensitive to the initial mass of the star. Stars with $M_{\rm ini} \lesssim 2\,M_\odot$ become

Downloaded from https://academic.oup.com/mnras/article/467/4/4431/3072233 by INAF Roma (Osservatorio Astronomico di Roma) user on 08 October 2020

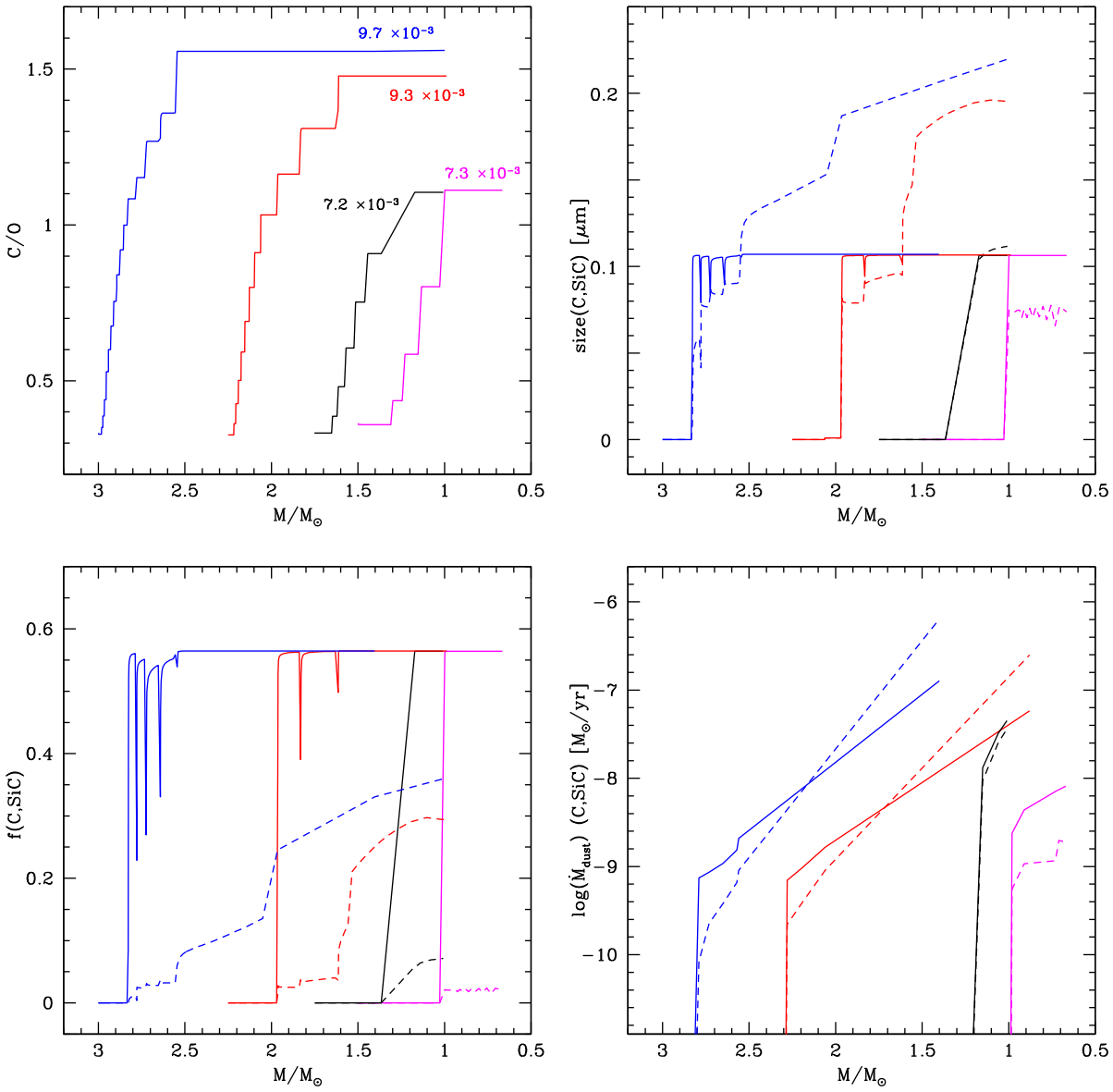

Figure 3. Variation during the AGB phase of the physical and dust properties of stars with initial mass in the range [1.5–3] $M_{\odot}$, shown by the coloured lines from magenta to blue. The current mass of the star (decreasing during the evolution) is displayed on the abscissa. The quantities shown in the four panels are: surface C/O ratio, with the values of the final surface carbon mass fraction also indicated (top-left), size of SiC and solid carbon grains (top-right, solid and dashed lines, respectively), fraction of silicon condensed into SiC and of carbon condensed into dust (bottom-left, solid and dashed lines, respectively), SiC and carbon mass-loss rates (bottom-right, solid and dashed lines, respectively). A coloured version of this plot is available online.

C-stars only in the very final AGB phases, with a surface C/O only slightly above unity (DC16; see also the top-left panel of Fig. 3). In these conditions, the excess of carbon with respect to oxygen is so small that the masses of SiC and solid carbon are very similar. On the other hand, in stars with $M_{\rm ini} > 2\,M_{\odot}$, we find that C/O ∼1.5 and the amount of carbon not locked into CO molecules is sufficiently large to allow the formation of solid carbon in excess of that of SiC.

4.3 Comparison with other AGB dust yields

In this section we focus attention on a comparison with different results on the AGB dust yields (i.e. the mass of the various dust species produced), obtained using the same methodology as for the dust formation model but a different AGB phase description.

As stated previously, we use the same approach as introduced for the first time by Ferrarotti & Gail (2006, hereinafter FG06) to describe the wind dynamics and dust production. FG06 base their modelling on a synthetic description of the AGB phase. The metallicity used by FG06 ($Z = 0.020$) is slightly higher than the value adopted here ($Z = 0.018$), but the difference is sufficiently small to allow a straight comparison of the results.

In Figs 2 and 4 we show FG06's dust yields, in order to allow a direct comparison with our results. The different parametrization adopted to describe the TDU efficiency is probably the reason for the difference in the minimum mass reaching the C-star stage, which is $2\,M_{\odot}$ in FG06, compared with $1.5\,M_{\odot}$ found in the present work, for models of solar metallicity. A common behaviour of the two sets of models is the increase in the amount of solid carbon and SiC produced with the initial mass. In the FG06 case, larger

Downloaded from https://academic.oup.com/mnras/article/467/4/4431/3072233 by INAF Roma (Osservatorio Astronomico di Roma) user on 08 October 2020

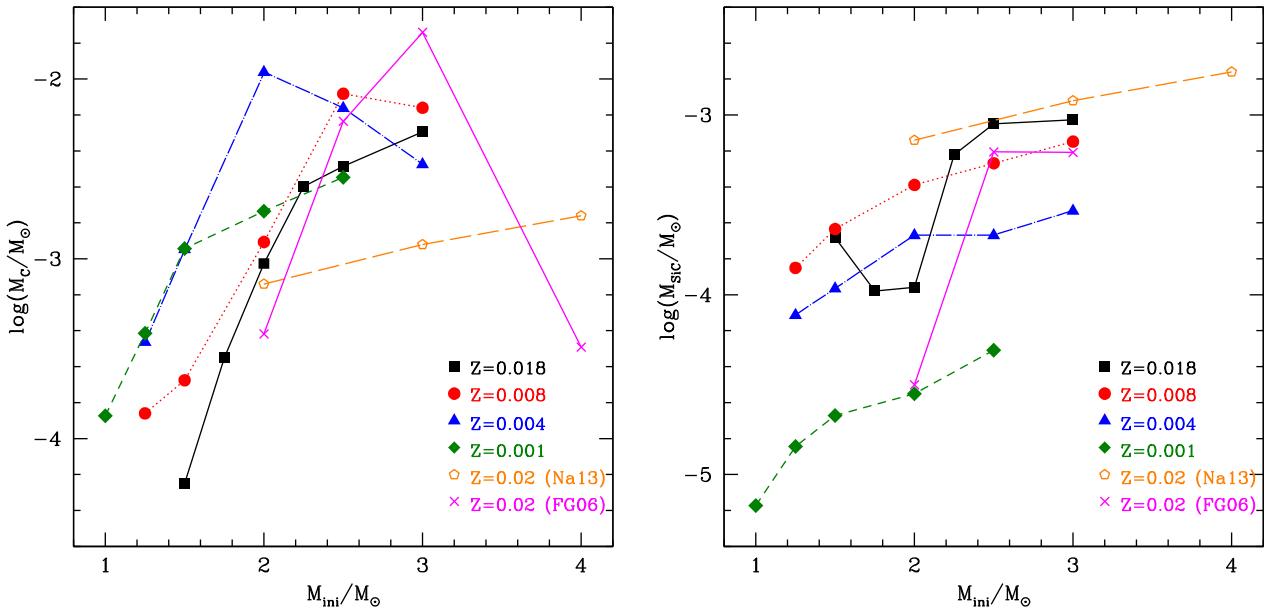

Figure 4. The mass of solid carbon (left panel) and silicon carbide (right panel) produced by solar-chemistry AGB stars of different masses compared with models of similar metallicity by Nanni et al. (2013, Na13) and Ferrarotti & Gail (2006, FG06) and with the results for lower-metallicity models ($Z = 10^{-3}$, 4×10^{-3} and 8×10^{-3}). The same symbols as in Fig. 2 are adopted.

quantities of solid carbon are found in the range of mass close to the lower threshold required to activate HBB; this is probably due to the larger number of thermal pulses experienced in the FG06 models, resulting in a larger amount of surface carbon available to form carbon dust. Stars with initial masses lower than $2\,M_\odot$ do not become C-stars, and are responsible for the production of silicate dust in the range $10^{-3} - 10^{-4}\,M_\odot$.

Regarding the massive star domain, FG06 assume that the HBB is active for $M \geq 4\,M_\odot$. While the production of silicates is comparable with our results in the lower limit of this range of masses, for the most massive AGB stars the amount of silicates formed is a factor of ∼2 smaller than that in the present models: this is due to the higher efficiency of the HBB process, in turn determined by the greater efficiency of the convective models adopted here. An additional difference between the present results and FG06 regarding the dust budget of massive stars is that in the latter models some carbonaceous dust is produced at the end of the AGB phase, owing to the effects of some late TDU events, after HBB is extinguished.

The same methodology as introduced by FG06, and used in the present work, was used also by Nanni et al. (2013, hereafter Na13), to calculate the dust yields from AGB stars with solar chemistry. For the sake of clarity, we compare the silicate total dust production with the low-condensation-temperature case (i.e. chemical sputtering case) adopted by Na13, which is the same approximation as considered in the present work. However, Na13 state that low- and high-condensation-temperature approaches reach approximately the same condensation degrees during the phases that dominate the total dust production.

The dust yields predicted by Na13 are shown in Figs 2 and 4. An obvious difference is the threshold mass that separates stars producing mainly carbonaceous dust from those producing silicate and alumina dust. This mass limit is $M_{\rm ini} \sim 3\,M_\odot$ in the present computation, while it is $M_{\rm ini} \sim 4\,M_\odot$ in Na13.

This difference stems from the different convection modellings. Our AGB computations are based on the Full Spectrum of Turbulence (FST) convective model (Canuto & Mazzitelli 1991). As shown by Ventura & D'Antona (2005), the use of FST modelling leads to very efficient HBB conditions; that is, the minimum mass required to experience HBB in the FST model is significantly lower than for other AGB models in the literature (e.g. Karakas & Lugaro 2016).

For massive AGB stars with $M_{\rm ini}$ in the range [5–6] $M_\odot$, the amounts of alumina and silicate dust predicted by Na13 are approximately a factor of 2 higher than in our AGB models (see Fig. 2). This difference is attributable mainly to the different duration of the highest-luminosity phase that is coupled with the maximum dust production phase. In Na13, this phase is a factor of ∼2 longer than in our AGB models. In the case of alumina dust, the choice of the sticking coefficients also affects this difference. We use $\alpha_{\rm Al_2O_3} = 0.1$, while Na13 adopted a much higher value of $\alpha_{\rm Al_2O_3} = 1$.

For low-mass AGB stars, the mass of SiC is similar in the two studies, while the amount of carbon dust produced by our models is approximately a factor of 2 larger than in Na13. This is probably because of the different choice adopted for the fraction of seed nuclei with respect to the number density of hydrogen molecules (ϵ_s). We follow Ferrarotti & Gail (2006) and assume that $\epsilon_s = 10^{-13}$, while Na13 assume that the number of seed particles relevant for the formation of carbon grains scales with C/O.

4.4 The total dust production from solar-metallicity AGB stars

Fig. 5 shows the total dust mass produced by AGB stars of solar metallicity. In order to better understand the trend of the dust mass with metallicity, we also show the results from our previous works focused on lower-Z AGB stars (Ventura et al. 2012a,b; Di Criscienzo et al. 2013; Ventura et al. 2014).

The dependence of the dust mass produced on the initial stellar mass can be understood on the basis of the arguments presented earlier in this section and can be summarized as follows.

(i) In low-mass AGB stars, the total amount of dust produced ($M_{\rm dust}$), composed of solid carbon and SiC, increases with the initial stellar mass. We find that $M_{\rm dust} \sim 5 \times 10^{-4}\,M_\odot$ for $M_{\rm ini} = 1.5\,M_\odot$,

Downloaded from https://academic.oup.com/mnras/article/467/4/4431/3072233 by INAF Roma (Osservatorio Astronomico di Roma) user on 08 October 2020

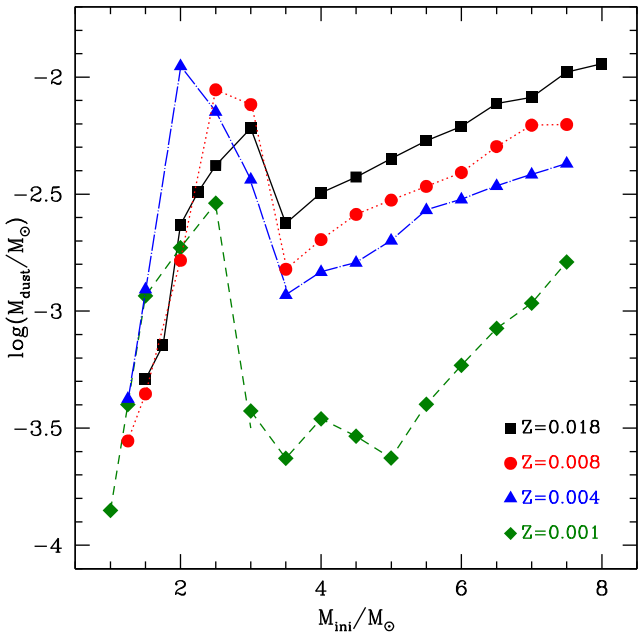

Figure 5. The total dust mass produced by solar-metallicity AGB models of various initial mass are indicated with black, full squares and are connected with a solid line. Also shown are the results for lower-metallicity models, with the same symbols as in Fig. 2.

and is up to $M_{\rm dust} \sim 6 \times 10^{-3}\,{\rm M}_{\odot}$ for $M_{\rm ini} = 3\,{\rm M}_{\odot}$. The reason for this is that the number of TDU events experienced increases with $M_{\rm ini}$. Consequently, higher-mass stars accumulate more carbon in the external regions, which favours the formation of carbon dust.

(ii) Regarding the dust composition, we find that for increasing $M_{\rm ini}$ the ratio between the mass of solid carbon and the mass of SiC increases. This is because the amount of SiC formed, unlike carbon, is rather independent of the surface chemical composition, as the most relevant species for the formation of SiC is silicon.

(iii) The AGB model forming the minimum amount of silicate dust, $M_{\rm dust} \sim 2.4 \times 10^{-3}\,{\rm M}_{\odot}$, has an initial mass $M_{\rm ini} = 3.5\,{\rm M}_{\odot}$. This is the lowest mass experiencing HBB, which destroys surface carbon, thus preventing the formation of carbonaceous dust. On the other hand, the production of silicates is low, because this star experiences a soft HBB during the AGB phase and the luminosity is below $25\,000 L_{\odot}$.

(iv) For massive AGB/SAGB stars, the mass of dust formed increases with $M_{\rm ini}$, ranging from the quantity given in the previous point (iii) to $M_{\rm dust} = 1.14 \times 10^{-2}\,{\rm M}_{\odot}$, for the most massive SAGB star with $M_{\rm ini} = 8\,{\rm M}_{\odot}$. This is because higher-mass stars experience a stronger HBB, and thus evolve at higher luminosities and mass-loss rates.

(v) For massive AGB/SAGB stars the majority of the dust formed is composed of silicates, with ∼10 per cent of alumina dust.

The dependence of dust production on the initial metallicity of massive AGB/SAGB stars is fairly straightforward. Dust production increases with Z, because the initial mass fractions of the key elements relevant to the formation of silicate and alumina dust (i.e. silicon and aluminium, respectively) increase almost linearly with Z, and their abundance does not change during the AGB evolution. The trend of the dust mass with Z is not completely linear though, because lower-Z AGB stars experience a more efficient HBB, which, for the reasons given above, favours a more efficient formation of silicates and of Al_2O_3.

For low-mass AGB stars, the dependence of dust production on the initial stellar metallicity is more complex. In these stars, most of the dust formed is composed of solid carbon, which is sensitive to the amount of carbon accumulated in the surface regions, as a consequence of repeated TDU episodes. Solar-metallicity AGB stars produce, on average, a smaller quantity of dust compared with their lower-metallicity counterparts. The reasons for this are twofold: (a) the C-star stage is reached later in the AGB evolution, when a significant fraction of the envelope has been lost; (b) the initial amount of oxygen in the star is larger, and thus a smaller quantity of carbon (in excess of oxygen) is available to form dust.

5 CONCLUSIONS

In this paper, we have completed the grid of ATON dust yields for AGB/SAGB stars, extending our previous calculations to solar-metallicity stars. Our main results can be summarized as follows.

The kind of dust produced reflects a dichotomy (C-rich versus O-rich) in the evolution of the surface chemical composition, which depends on the initial stellar mass, $M_{\rm ini}$.

In low-mass AGB stars, with $1.5\,{\rm M}_{\odot} \leq M_{\rm ini} \leq 3\,{\rm M}_{\odot}$, the surface chemical composition is altered by the several TDU episodes that eventually lead to the formation of a C-star (C/O > 1). The formation of solid carbon and SiC grains takes place in the circumstellar envelope of these stars. The size of SiC grains formed stays at around $a_{\rm SiC} \sim 0.1\,\mu{\rm m}$ for the whole AGB life. However, the size of carbon grains increases with the increasing amount of carbon being accumulated in the surface regions. The carbon dust particles with the largest sizes, $a_{\rm C} \gtrsim 0.2\,\mu{\rm m}$, are formed in the very final evolutionary phases of AGB stars with $M_{\rm ini} = 2.5$–$3\,{\rm M}_{\odot}$. The mass of carbonaceous dust formed increases with the mass of the star, ranging from a few $10^{-4}\,{\rm M}_{\odot}$ for $M_{\rm ini} \sim 1.5\,{\rm M}_{\odot}$, to $\sim 10^{-3}\,{\rm M}_{\odot}$ for $M_{\rm ini}$ ∼2.5–3 ${\rm M}_{\odot}$. In the lowest-mass stars, the dominant dust component is SiC, while in their more massive counterparts most of the dust produced is in the form of solid carbon.

Massive AGB/SAGB stars with $M_{\rm ini} > 3\,{\rm M}_{\odot}$ experience HBB. In this case the formation of carbon stars is inhibited by the destruction of surface carbon via proton-capture reactions at the base of the convective envelope. The most relevant dust species formed in these stars are silicate and alumina dust. The latter is more stable than silicates, but the amount of dust that can be produced is severely limited by the scarcity of aluminium. Alumina grains grow until reaching dimensions of the order of $a_{\rm Al_2O_3} \sim 0.06$–$0.07\,\mu{\rm m}$. Most of the dust produced by massive AGB/SAGB stars is in the form of silicates. The size reached by the dominant silicates grains (i.e. olivine) is in the range $0.1 < a_{\rm ol} < 0.15\,\mu{\rm m}$. The mass of dust produced increases with $M_{\rm ini}$ because higher-mass stars evolve on more massive degenerate cores and are exposed to stronger HBB conditions. We find that $M_{\rm dust} \sim 3.4 \times 10^{-3}\,{\rm M}_{\odot}$ for $M_{\rm ini} \sim 3.5\,{\rm M}_{\odot}$, up to a maximum of $M_{\rm dust} \sim 1.1 \times 10^{-2}\,{\rm M}_{\odot}$ for $M_{\rm ini} \sim 8\,{\rm M}_{\odot}$. Silicates are the largely dominant dust species in all cases.

Previously computed ATON AGB models with dust formation have been able to explain and interpret photometric observations of evolved stars in several low-metallicity galaxies of the LG. The results of the present study will allow these studies to be extended to evolved stellar populations in our Galaxy and other high-metallicity LG galaxies. In addition, the complete grid of dust and metal yields based on ATON AGB/SAGB models with metallicity $0.001 \leq Z \leq 0.018$ and initial mass $1.5\,{\rm M}_{\odot} \leq M_{\rm ini} \leq 8\,{\rm M}_{\odot}$ will be a valuable tool for chemical evolution studies, allowing estimation of the contribution of intermediate-mass stars to metal and dust enrichment on time-scales >40 Myr. In a more general context, the

Downloaded from https://academic.oup.com/mnras/article/467/4/4431/3072233 by INAF Roma (Osservatorio Astronomico di Roma) user on 08 October 2020

solar-metallicity AGB dust yields will allow a comparison of the relative roles of AGB and SNe as stellar sources of dust over a wide range of metallicity, and an assessment of the contribution of AGB stars to the existing dust mass of the Milky Way, complementing the work that has already been carried out on the Magellanic Clouds.

ACKNOWLEDGEMENTS

DAGH was funded by the Ramón y Cajal fellowship number RYC-2013-14182. DAGH and FD acknowledge support provided by the Spanish Ministry of Economy and Competitiveness (MINECO) under grant AYA-2014-58082-P. RS and RV acknowledge funding from the European Research Council under the European Unions Seventh Framework Programme (FP/2007-2013)/ERC Grant Agreement no. 306476. MDC acknowledges the contribution of the FP7 SPACE project ASTRODEEP (ref. no. 312725), supported by the European Commission.

REFERENCES

Blöcker T., Schöenberner D., 1991, A&A, 244, L43
Bocchio M., Marassi S., Schneider R., Bianchi S., Limongi M., Chieffi A., 2016, A&A, 587, 157
Bruno C. G. et al., 2016, Phys. Rev. Lett. 117, 142502
Canuto V. M. C., Mazzitelli I., 1991, ApJ, 370, 295
Cristallo S., Straniero O., Gallino R., Piersanti L., Dominguez I., Lederer M. T., 2009, ApJ, 696, 797
Cristallo S., Straniero O., Piersanti L., Gobrecht D., 2015, ApJS, 219, 40
Dell'Agli F., García Hernández D. A., Rossi C., Ventura P., Di Criscienzo M., Schneider R., 2014a, MNRAS, 441, 1115
Dell'Agli F., Ventura P., García Hernández D. A., Schneider R., Di Criscienzo M., Brocato E., D'Antona F., Rossi C., 2014b, MNRAS, 442, L38
Dell'Agli F., Ventura P., Schneider R., Di Criscienzo M., García-Hernández D. A., Rossi C., Brocato E., 2015a, MNRAS, 447, 2992
Dell'Agli F., García-Hernández D. A., Ventura P., Schneider R., Di Criscienzo M., Rossi C., 2015b, MNRAS, 454, 4235
Dell'Agli F., Di Criscienzo M., Boyer M. L., García-Hernández D. A., 2016, MNRAS, 460, 4230
Di Criscienzo M. et al., 2013, MNRAS, 433, 313
Di Criscienzo M., Ventura P., García-Hernández D. A. et al., 2016, MNRAS, 462, 395
Doherty C. L., Gil-Pons P., Lau H. H. B., Lattanzio J. C., Siess L., 2014, MNRAS, 437, 195
Ferrarotti A. D., Gail H. P., 2001, A&A, 371, 133
Ferrarotti A. D., Gail H. P., 2002, A&A, 382, 256
Ferrarotti A. D., Gail H. P., 2006, A&A, 553, 576
Gail H. P., Sedlmayr E., 1985, A&A, 148, 183
Gail H. P., Sedlmayr E., 1999, A&A, 347, 594
García-Berro E., Iben I. J., 1994, ApJ, 434, 306
García-Berro E., Ritossa C., Iben I. J., 1997, ApJ, 485, 765
Javadi A., van Loon J. Th., Mirtorabi M. T., 2011a, MNRAS, 411, 263
Javadi A., van Loon J. Th., Mirtorabi M. T., 2011b, MNRAS, 414, 3394
Javadi A., van Loon J. Th., Khosroshahi H., Mirtorabi M. T., 2015, MNRAS, 432, 2824
Jones O. C., McDonald I., Rich R. M., Kemper F., Boyer M. L., Zijlstra A. A., Bendo G. J., 2015, MNRAS, 446, 1584
Karakas A. I., 2010, MNRAS, 403, 1413
Karakas A. I., 2014, MNRAS, 445, 347
Karakas A. I., Lattanzio J. C., 2014, PASA, 31, e030
Karakas A. I., Lugaro M., 2016, 825, 26
Lugaro M. et al., 2017, Nat. Astron., 1, 0027
McQuinn K. B. W. et al., 2007, ApJ, 664, 850
Mancini M., Schneider R., Graziani L., Valiante R., Dayal P., Maio U., Ciardi B., Hunt L. K., 2015, MNRAS, 451, L70
Mancini M., Schneider R., Graziani L., Valiante R., Dayal P., Maio U., Ciardi B., 2016, MNRAS, 462, 3130
Marassi S., Chiaki G., Schneider R., Limongi M., Omukai K., Nozawa T., Chieffi A., Yoshida N., 2014, ApJ, 794, 100
Marassi S., Schneider R., Limongi M., Chieffi A., Bocchio M., Bianchi S., 2015, MNRAS, 454, 4250
Marigo P., 2002, A&A, 387, 507
Marigo P., Ripamonti E., Nanni A., Bressan A., Girardi L., 2016, MNRAS, 456, 23
Mould J., Barmby P., Gordon K., Willner S. P., Ashby M. L. N., Gehrz R. D., Humphreys R., Woodward C. E., 2008, ApJ, 687, 230
Nanni A., Bressan A., Marigo P., Girardi L., 2013, MNRAS, 434, 2390
Nanni A., Bressan A., Marigo P., Girardi L., 2014, MNRAS, 438, 2328
Nanni A., Marigo P., Groenewegen M. A. T., Aringer B., Girardi L., Pastorelli G., Bressan A., Bladh S., 2016, MNRAS, 462, 1215
Paczynski B., 1970, Acta Astron., 20, 47
Renzini A., Voli M., 1981, A&A, 94, 175
Schneider R., Valiante R., Ventura P., dell'Agli F., Di Criscienzo M., Hirashita H., Kemper F., 2014, MNRAS, 442, 1440
Sharp C. M., Huebner W. F., 1990, ApJS, 72, 417
Siess L., 2006, A&A, 448, 717
Siess L., 2007, A&A, 476, 893
Siess L., 2009, A&A, 497, 463
Siess L., 2010, A&A, 512, 10
Takigawa A., Tachibana S., Nagahara H., Ozawa K., 2015, ApJS., 218, 1
Valiante R., Schneider R., Bianchi S., Andersen A. C., 2009, MNRAS, 397, 1661
Valiante R., Schneider R., Salvadori S., Bianchi S., 2011, MNRAS, 416, 1916
Ventura P., D'Antona F., 2005, A&A, 431, 279
Ventura P., Marigo P., 2009, MNRAS, 399, L54
Ventura P., Marigo P., 2010, MNRAS, 408, 2476
Ventura P. et al., 2012a, MNRAS, 420, 1442
Ventura P. et al., 2012b, MNRAS, 424, 2345
Ventura P., Di Criscienzo M., Carini R., D'Antona F., 2013, MNRAS, 431, 3642
Ventura P., Dell'Agli F., Schneider R., Di Criscienzo M., Rossi C., La Franca F., Gallerani S., Valiante R., 2014, MNRAS, 439, 977

This paper has been typeset from a TEX/LATEX file prepared by the author.

Downloaded from https://academic.oup.com/mnras/article/467/4/4431/3072233 by INAF Roma (Osservatorio Astronomico di Roma) user on 08 October 2020